



HAL
open science

Sidewall passivation layer thickness and composition profiles of etched silicon patterns from angle resolved x-ray photoelectron spectroscopy analysis

Moritz Haass, Maxime Darnon, Olivier Joubert

► **To cite this version:**

Moritz Haass, Maxime Darnon, Olivier Joubert. Sidewall passivation layer thickness and composition profiles of etched silicon patterns from angle resolved x-ray photoelectron spectroscopy analysis. Journal of Applied Physics, 2012, 111 (12), pp.111-124905. 10.1063/1.4729775 . hal-00755597

HAL Id: hal-00755597

<https://hal.science/hal-00755597>

Submitted on 5 Jan 2024

HAL is a multi-disciplinary open access archive for the deposit and dissemination of scientific research documents, whether they are published or not. The documents may come from teaching and research institutions in France or abroad, or from public or private research centers.

L'archive ouverte pluridisciplinaire **HAL**, est destinée au dépôt et à la diffusion de documents scientifiques de niveau recherche, publiés ou non, émanant des établissements d'enseignement et de recherche français ou étrangers, des laboratoires publics ou privés.

Sidewall passivation layer thickness and composition profiles of etched silicon patterns from angle resolved x-ray photoelectron spectroscopy analysis

Moritz Haass,^{a)} Maxime Darnon, and Olivier Joubert

CNRS/UJF-Grenoble1/CEA LTM, 17 avenue des Martyrs, 38054 Grenoble cedex 9, France

(Received 12 March 2012; accepted 17 May 2012; published online 20 June 2012)

In this study, we present a technique to analyze side wall passivation layers formed on silicon sidewalls after plasma processing. The thickness and chemical composition are derived from angle resolved x-ray photoelectron spectroscopy analyses. It is a non-destructive, quasi *in situ* method to determine profiles of the thickness and the chemical composition of passivation layers in trenches up to an aspect ratio of about 3. The performance of this technique to quantify the passivation layer thickness is compared to a standard technique using secondary electron microscopy images with respect to two different samples and is found to be at least equivalent. The possible uncertainties and limitations of this technique are discussed as well. © 2012 American Institute of Physics.

[<http://dx.doi.org/10.1063/1.4729775>]

I. INTRODUCTION

The continuous downscaling in the microelectronics industry imposes increasing demands for the pattern transfer, e.g., in terms of critical dimension (CD) control. Plasma processes can decrease (e.g., resist “cure” and resist trimming processes) or increase (non-vertical etch slope in silicon) the CD. One important factor of the CD variation during etch processes is the formation of the sidewall passivation layer (SPL) that protects the structures from lateral etching.^{1–3} Hence, the control of the SPL is essential to achieve the correct final pattern dimensions. Unfortunately, it is rather difficult to analyze SPLs in terms of thickness and chemical composition without air exposure in order to understand their formation. The most common way to measure the SPL thickness profile is the use of cross section images obtained from secondary or transmission electron microscopy (SEM/TEM) measurements.^{4,5} This destructive *ex situ* technique compares the etched profiles before and after an additional wet clean, which selectively removes the SPL (the thickness profile can be estimated from the differences). In this case, it is very important to analyze always the same part of the pattern because of small differences between different lines. Thus, this technique gives only limited (if not no) information of the average SPL thickness throughout the pattern. A very powerful technique to study passivation layers is the combination of TEM and electron energy loss spectroscopy (EELS).⁶ It allows highly accurate measurements of the SPL profile and gives additional information on its chemical composition. Disadvantages are the air exposure and the large amount of time needed for preparation and measurement.

Other studies use non-destructive three-dimensional atomic force microscopy (3D-AFM) to measure the SPL thickness.^{7–9} But since this technique uses a rather large tip, it is not suitable for small trench sizes below 100 nm.

The chemical composition of the SPL is often studied by x-ray photoelectron spectroscopy (XPS).^{1,6,7,10–15} A

homogeneous pattern of lines and trenches is perpendicularly analyzed by an XPS system so that the signals from the trench bottom and part of the sidewalls are shadowed by adjacent sidewalls. The signal from the mask is identified thanks to a technique of differential charging: an electron flood gun charges dielectric materials and shifts their peak positions (binding energies) in the XPS spectra.¹⁶

In principle, it is also possible to estimate the thickness of a thin overlayer (OL) on a substrate from XPS measurements.^{17–21} Following this method, Pargon *et al.*²² compared the XPS signal of a blanket resist layer to the signal of a resist pattern and calculated the signal from the sidewall by subtraction. This way they could estimate the average SPL thickness, but no profile of the SPL was obtained.

In this study, we report the development of a non-invasive angle-resolved XPS (ARXPS) technique that provides at the same time profiles of the SPL thickness and profiles of the chemical composition. The quasi *in situ* analysis allows us to investigate the passivation layer directly after the etch process without exposure to air. Two examples with different SPL thicknesses are presented and compared to SEM measurements. Possible errors and limitations of this technique are also discussed.

II. TECHNIQUE

A. Thickness analysis of a single overlayer

ARXPS data are frequently used not only to analyze the chemical composition but also to determine the thickness of an overlayer on a substrate. Cumpson and Seah¹⁷ describe in detail how to calculate the thickness using intensity ratios for a simple homogeneous overlayer on a substrate S. If signals from the same elements in OL and S (e.g., SiO₂ on Si) are used, the thickness can be expressed by

$$d = \lambda \cos(\theta) \ln \left[1 + \frac{I_{OL}}{I_S} \cdot \frac{1}{R_0} \right], \quad (1)$$

^{a)}moritz.haass@cea.fr.

where $R_0 = I_{OL}^\infty / I_S^\infty$, I_i^∞ is the intensity of an infinite specimen i of substrate or overlayer material, d is the overlayer thickness, λ is the attenuation length of the photoelectrons in the overlayer, and θ is the emission/detection angle of the photoelectrons. Several authors have provided theoretical calculations (fitted to experimental data) to calculate the attenuation length, depending on the density, stoichiometry, and in some cases also the electronic bandgap^{17,18,21} of the materials. The stoichiometry (mean atomic number Z and mean atomic mass μ) can be extracted from the chemical composition measured by XPS without taking into account the possible hydrogen contribution. The other parameters remain more or less unknown in our case. Since our XPS data of the SPL indicate a bromine rich silicon oxide layer, we approximate the density and bandgap by tabulated values of SiO₂. By applying the most used set of equations, published by Tanuma, Powell, and Penn (TPP-2M),^{18,19} we obtain an attenuation length of $\lambda = 3.367$ nm. Similarly, R_0 can be calculated or obtained experimentally as shown, e.g., by Seah and Spencer²³ who advise to take rather the measured value than the theoretical value for thickness calculations. Therefore, we use a value of $R_0 = 0.778$ for the thickness calculation, obtained from preliminary experiments on SiO₂.

B. Thickness of sidewall passivation layers

This technique can also be used to determine the thickness of a SPL directly after the etch process. In order to reduce the signal to noise ratio, it is necessary to collect as much signal as possible originating from the sidewalls. For this purpose, a pattern consisting of lines and trenches with equal widths is very convenient. This pattern should be larger than the x-ray spot size from the ARXPS system and needs to be positioned in such a way that the plane of detection of the ARXPS system is perpendicular to the orientation of the trenches. Thus, the average XPS signal originates both from the mask and the pattern sidewalls (Fig. 1). Each detection angle θ corresponds to a different observed area of the

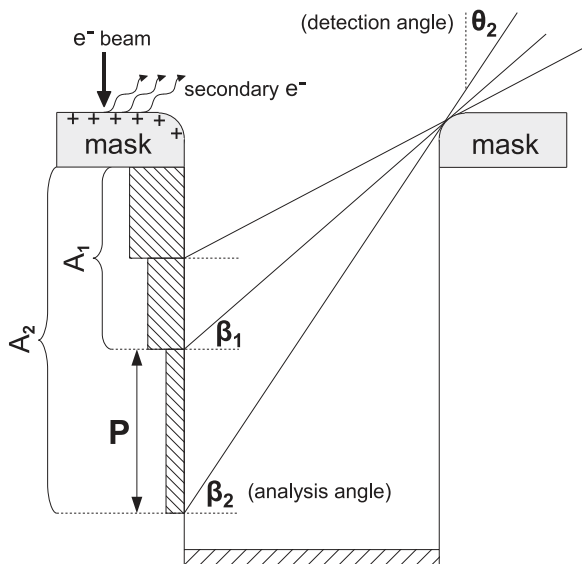


FIG. 1. Sketch of the XPS technique.

SPL, while the signal from the rest of the SPL and from the trench bottom never reach the detector since they are obstructed from the detector by adjacent lines. For large detection angles, all photo-electrons from the SPL are blocked and the measured signal originates only from the mask. Therefore, the number of data points for the SPL is reduced, especially for thinner trenches. The detection angle defines also the maximal aspect ratio that can be analyzed. The aspect ratio is the ratio of the probed trench depth (including the mask) over its width. It is a more convenient parameter to use if trenches with different widths are studied.

In a second step, the SPL signal has to be isolated from the mask signal. This can easily be done, if the pattern stack consists of a dielectric mask (e.g., SiO₂) on top of a conducting bulk material (e.g., trenches in bulk silicon). In this case, it is possible to charge the dielectric mask separately from the trench walls, which results in a shift of the binding energies in the mask material. Consequently, the peak positions from the mask signal in the XPS spectra are also shifted.¹⁶ The differential charging is carried out by applying an electron beam dedicated to neutralize accumulated charges on dielectric surfaces. Depending on the electron beam energy, the mask can be charged either negatively due to an accumulation of negative charges (low energy beam) or positively due to the loss of secondary electrons (high energy beam). A positive mask charge shifts the XPS peaks to higher binding energies and vice versa.²⁴

The extracted signal gives information on the average chemical composition (without hydrogen, which cannot be detected by XPS) of the SPL of the measured area along the trench sidewall. The average SPL thickness is calculated with Eq. (1).

Using the average thickness and chemical composition, it is possible to obtain the signal intensities from each part P of the sidewall using the angle resolution of the XPS system (see Fig. 1). P is defined as the area that is observed additionally going from a rather flat detection angle (θ_1) to a steeper angle (θ_2). However, the signal intensities of the observed sidewall areas (A_1 and A_2) at different angles cannot be subtracted directly to obtain the signal from P due to their dependence on the detection angle.¹⁷ Thus, it is necessary to calculate the theoretical signal from area A_1 at the detection angle θ_2 . Taking this into account, we can estimate the substrate and overlayer signal intensities of part P of the SPL,

$$I_{OL,P}^{\theta_2} = I_{OL,A_2}^{\theta_2} - I_{OL,A_1}^{\theta_1} \cdot \frac{1 - \exp[-d_1/\lambda \cos(\beta_2)]}{1 - \exp[-d_1/\lambda \cos(\beta_1)]} \quad (2)$$

and

$$I_{S,P}^{\theta_2} = I_{S,A_2}^{\theta_2} - I_{S,A_1}^{\theta_1} \cdot \frac{\exp[-d_1/\lambda \cos(\beta_2)]}{\exp[-d_1/\lambda \cos(\beta_1)]}, \quad (3)$$

where the emission angle β_i is defined with respect to the surface normal so that $\beta_i = 90^\circ - \theta_i$ (assuming a vertical trench sidewall). From the obtained signal intensities, the chemical composition and the thickness can be calculated for each part P of the sidewall, resulting in a profile along the sidewalls.

III. UNCERTAINTIES AND LIMITATIONS

A. Assumptions and possible errors

Although this technique proves to be quite accurate, as shown later, we still need to keep in mind the assumptions that are made to determine the SPL thickness and the possible errors that they imply.

- (1) We need to assume that the XPS measurement procedure itself results in reliable data. Seah²⁵ evaluated uncertainties in thickness measurements using XPS for ultrathin SiO₂ on Si and reported an uncertainty of 0.4 nm over the range $2.5 < d < 7.8$ nm only due to the analysis procedure and hardware. However, since the data are always obtained in the same system, the relative change between different samples should be unaffected.
- (2) Furthermore, we assume the presence of vertical sidewalls. In our case, the sidewall slope is changing by not more than 3° (from the vertical case) between trench top and bottom. Nevertheless, this leads to an error in the thickness estimation of between 2% and 14%, depending on the detection angle (see Eq. (1)).
- (3) Also, we use a simple bi-layer model where the overlayer is treated as a homogeneous material. Since the formation of the passivation layer is a continuous process in a rather stable environment, this assumption might be quite accurate; but due to a lack of information on the SPL, we can neither validate it at this point nor estimate an error.
- (4) The attenuation length λ is calculated using the stoichiometry of the XPS measurement as well as the density and the bandgap data from SiO₂, due to the lack of information on the bromine rich silicon oxide passivation layer. For the same reason, R_0 is determined experimentally for SiO₂. Seah and Spencer²³ discuss in detail the errors in the determination of a thin SiO₂ overlayer thickness, which are related to theoretical and experimental values of R_0 and λ . They cite a variation of R_0 between 0.67 and 0.87 for previously published experimental values. In addition, they determine themselves R_0 experimentally and theoretical and find values of 0.88 and 0.53, respectively. Regarding the attenuation length λ , they report an agreement between the theoretical and experimental values within an error of 10%. Other studies state a root mean square deviation of the estimated values from experimentally obtained attenuation lengths in a range between 1% and 20%,^{19,20} depending on the probed materials and the used material properties. Moreover, the experimental results presented later indicate that the chemical composition changes slightly with the aspect ratio (but not significantly with the trench width) which decreases additionally the confidence in R_0 and λ .

Considering all the above, we estimate the corresponding uncertainties by very conservative values, namely, by $R_0 = 0.778 \pm 0.30$ and $\lambda = 3.367 \pm 0.7$ nm. These values lead to an uncertainty of the thickness of 21%–28% (depending on the ratio of I_{OL}/I_S) and 20%, respectively. It should be mentioned that an error in λ results only in a constant offset

for all sets of data points and, thus, the relative behavior should remain unaffected.

The resulting probable total error is calculated to 29%–40% by using the Gaussian error propagation.

B. Limitations

The presence of both a dielectric mask and a conducting sidewall is necessary to charge the mask differentially in order to distinguish between the two signals. For large detection angles (small angle with respect to the sidewall surface), the photoelectron refraction will increasingly disturb the XPS measurement^{17,26} so that the maximal analyzable aspect ratio is approximately 3. Also, for SPL thicknesses larger than ~ 10 nm, the signal originating from the substrate is too small to estimate the thickness. Furthermore, it is necessary to have access to the relevant hardware, namely, the quasi *in situ* XPS system and adequate pattern structures. Finally, the time of acquisition for one pattern is quite high and ranges in the order of 2 h, depending on the signal to noise ratio. Despite these limitations, we think that this technique is a powerful method to analyze accurately the SPL.

IV. EXPERIMENTAL DETAILS

This technique is used here to study the sidewall passivation layer formed during the plasma etching of silicon trenches with a single layer hard mask of 50 nm silicon oxide in an HBr/O₂ chemistry. Each analyzed pattern consists of lines and approximately 300 nm deep trenches with equal widths. The lines are patterned by electron beam lithography and form areas of 1 mm \times 1 mm.

The etch experiments are carried out in a commercially available 300 mm AdvantEdgeTM DPS etch tool from Applied Materials, Inc. The plasma is sustained by two antenna coils, powered at 13.56 MHz, while the chuck is biased via a capacitively coupled RF power source, likewise working at 13.56 MHz. The power supply is modified with the PulsyncTM system to allow pulsing of the source and bias power with frequencies between 100 Hz and 20 kHz and duty cycles between 10% and 90%. More details about the reactor can be found in the literature.²⁷ By using the pulsing capability, we are able to change the SPL compared to a standard continuous wave (CW) process in order to verify the performance of our technique.

The angle resolved XPS measurements are performed in a customized Thermo Electron Theta 300 spectrometer which is connected to the etch reactor via a vacuum transfer system.²⁸ The XPS system is equipped with a high resolution monochromatic Al K α source at 1486.6 eV. For our experiments we used 8 different nominal detection angles ranging from 23.5° to 72.5° referred to the normal of the wafer, each with an acceptance angle of $\pm 3.50^\circ$. The x-ray spot size was set to 400 μ m, which is small compared to the size of the pattern area and the acceptance spot size of the detector (for all angles). Thanks to the laser aligner from the etch tool the orientation of the wafer can be controlled with a precision better than 2°. Moreover, the spectrometer is equipped with an electron beam system for charge neutralization. The electron beam energy is set to 300 eV in order to charge the dielectric

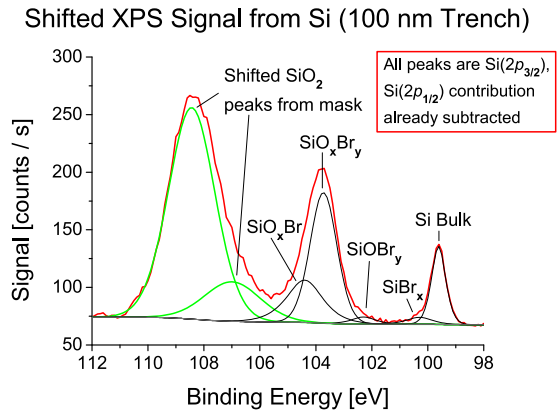


FIG. 2. XPS signal from Si: the signal from the oxide mask is shifted to the left towards higher binding energies due to the secondary electrons produced from an electron beam with an energy of 300 eV.

mask positively due to the loss of secondary electrons. This results in a shift of the peaks of the thin oxide mask of around 4–6 eV towards higher binding energies, as shown in Fig. 2 for the Si signal. In this figure, the $\text{Si}(2p_{1/2})$ contribution of each designated double peak was subtracted beforehand to simplify the identification of the peaks. After identifying the shifted contribution of the mask, it can be removed so that only the signal from the sidewalls remains.

V. RESULTS

In Fig. 3(a), the local thickness from each part P of the sidewall is shown for several trench widths. The XPS data for the 50 nm trenches, which are shown in the other graphs, were not acquired for the profiles from the CW experiment. We observe that the SPL thickness profile only depends on the aspect ratio but neither on the probed trench depth nor on

the trench width. With a larger aspect ratio, the SPL thickness decreases, principally due to the reduced collection angle of etch by-products from the gas phase that form the SPL. Also, the reduced exposure time of the SPL to the etch plasma with increased trench depth might play a role. However, since we observe no dependence of the SPL thickness on the trench depth only, the exposure time is thought to be a minor factor.

Another aspect, showing the accuracy of the technique, is the decrease of the SPL thickness for small aspect ratios (top of the trenches). The analyzed samples were etched in a process that leads to a strong mask faceting, leaving the top of the sidewalls less protected by the mask. Consequently, the top of the patterns are partly etched and we expect to see a thinner SPL on the surface which is in very good agreement with the presented XPS data. A similar profile was also found by Detter *et al.*⁵

In order to further verify the results from the ARXPS analysis, we used a SEM to measure the SPL from cross-sections of the trenches. The SPL can be removed in a short bath in HF so that the thickness can be obtained from measurements before and after HF application.^{4,5}

Unfortunately, this technique is not very accurate. First, the resolution of the SEM used in this study is not better than 3 nm. Moreover, only a very limited part of the pattern can be observed with a cross-section. This makes the measurement only a random sample and the real average for the whole pattern remains unknown. Nevertheless, the SEM images can give us an estimation of the absolute SPL thickness and its evolution with changing aspect ratio.

In Fig. 3(b), the results from the SEM analysis are shown for comparison. Although the SPL thickness for a specific aspect ratio seems to depend also on the trench

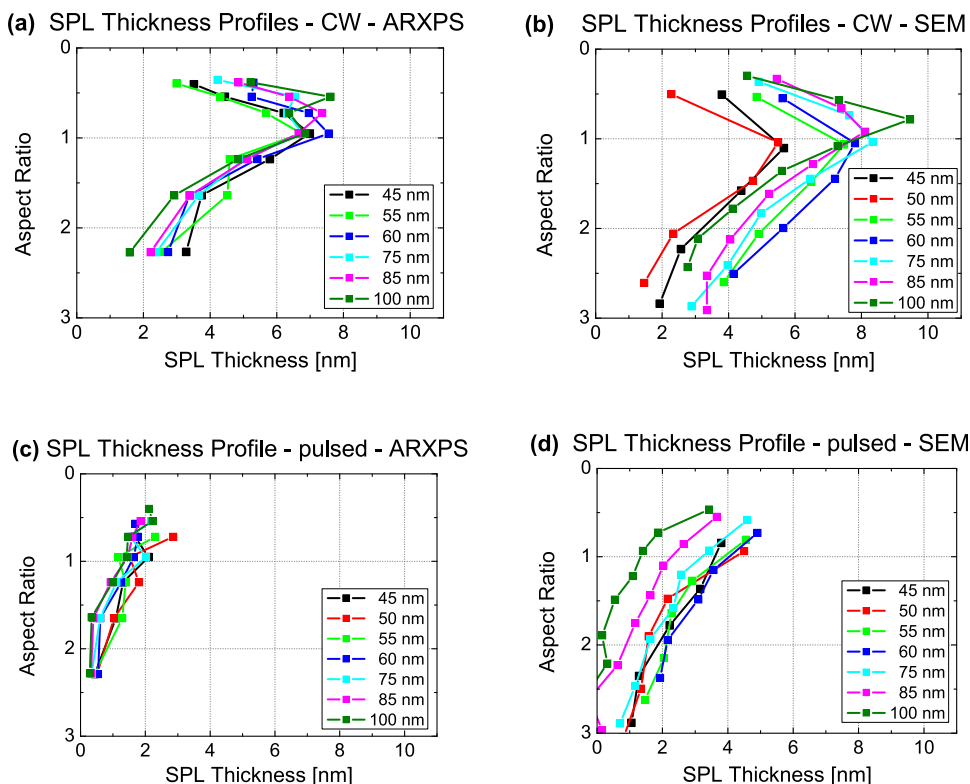


FIG. 3. Layer thickness profiles for different trench widths obtained from ARXPS (a) and (c) and SEM (b) and (d) measurements.

width, we do not observe any definite trend (e.g., thinner SPL thickness in thinner trenches). Thus, we attribute this variation to the large error in the SEM analysis technique. Still, the absolute values of the SPL thickness as well as the thickness profile are in very good agreement, validating R_0 and the parameters used to calculate the attenuation length.

In a next step, we etched another pattern in the same process, but instead of a continuous wave RF voltage, we used a pulsed process to decrease the SPL thickness. Details to the SPL thickness reduction in pulsed processes will be discussed in a following article. In Figs. 3(c) and 3(d), the results from the XPS technique and the SEM calculations are shown. The XPS analysis indicates an SPL thickness of less than 2 nm for most of the probed area which is inside the resolution limit of 3 nm of the SEM. This could explain the offset to slightly larger values for the SEM measurements. Still, both results are in good agreement, considering the large error for the SEM data. For a concluding evaluation of the XPS results a comparison to a more accurate technique like TEM would be necessary.

Fig. 4 shows the atomic percentage of bromine in the SPL from the CW case versus the aspect ratio of the investigated trench section for different trench widths. The amount of bromine is clearly dependent on the aspect ratio, but the variation is too large to identify any dependence on the trench CD. This is also true for the other elements present in the SPL, namely, silicon and oxygen. Therefore, we average the chemical compositions for each aspect ratio (part P) over the range of trench CDs. In Fig. 5, the entire averaged chemical composition of the SPL versus the probed aspect ratio is presented without the contribution of the bulk silicon for the CW experiment. We observe that with increasing aspect ratio the amount of oxygen in the SPL decreases and the amount of bromine increases. This is probably also linked to the change in collection angle of species from the gas phase, which is necessary to form the passivation layer. We believe that oxygen plays in this case the major role. With a larger collection angle, equivalent to a smaller aspect ratio, the oxygen flux increases and can further oxidize the SPL.^{3,12} More details on the formation of the passivation layers in HBr/O₂ plasmas will be presented in a following article.

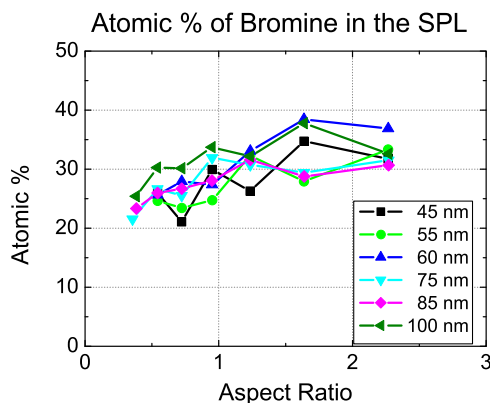


FIG. 4. Evolution of the bromine contribution in the SPL from the CW experiment for different aspect ratios and trench widths.

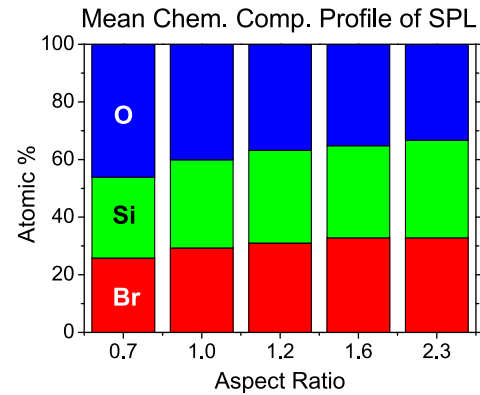


FIG. 5. Chemical composition of the SPL from the CW experiment with respect to the aspect ratio: averaged data from all trench widths. The contribution of the bulk silicon is removed.

VI. SUMMARY

We have presented a non-destructive quasi *in situ* technique to investigate the sidewall passivation layer after etching, giving a determination of the thickness and the chemical composition up to an aspect ratio of about 3. Thanks to the angle resolved resolution of the XPS system, it is possible to calculate profiles of both the thickness as well as the chemical composition without previous air exposure. The comparison with SEM measurements for two processes with very different deposited SPLs show a very good agreement between both techniques for the determination of the thicknesses.

ACKNOWLEDGMENTS

This work was supported by the French Government program “Investissements d’Avenir” managed by the National Research Agency (ANR) under the Contract No. ANR-10-EQPX-33 and by the European EUREKA/CATRENE program in the frame of the CT206 UTTERMOST project. Furthermore, we would like to thank Mickael Martin for the electron beam lithography.

¹E. Pargon, M. Darnon, O. Joubert, T. Chevolleau, L. Vallier, L. Mollard, and T. Lill, *J. Vac. Sci. Technol. B* **23**, 1913 (2005).

²G. S. Oehrlein and Y. Kurogi, *Mater. Sci. Eng. R* **24**, 153 (1998).

³S. Hamaguchi and M. Dalvie, *J. Vac. Sci. Technol. A* **12**, 2745 (1994).

⁴M. Tuda, K. Shintani, and H. Ootera, *J. Vac. Sci. Technol. A* **19**, 711 (2001).

⁵X. Detter, R. Palla, I. Thomas-Boutherin, E. Pargon, G. Cunge, O. Joubert, and L. Vallier, *J. Vac. Sci. Technol. B* **21**, 2174 (2003).

⁶L. Desvoivres, L. Vallier, and O. Joubert, *J. Vac. Sci. Technol. B* **19**, 420 (2001).

⁷O. Luere, E. Pargon, L. Vallier, B. Pelissier, and O. Joubert, *J. Vac. Sci. Technol. B* **29**, 011028 (2011).

⁸G. Dahlen, M. Osborn, N. Okulan, W. Foreman, A. Chand, and J. Foucher, *J. Vac. Sci. Technol. B* **23**, 2297 (2005).

⁹J. Thiault, J. Foucher, J. H. Tortai, O. Joubert, S. Landis, and S. Pauliac, *J. Vac. Sci. Technol. B* **23**, 3075 (2005).

¹⁰F. H. Bell, O. Joubert, and L. Vallier, *J. Vac. Sci. Technol. B* **14**, 1796 (1996).

¹¹K. V. Guinn, C. C. Cheng, and V. M. Donnelly, *J. Vac. Sci. Technol. B* **13**, 214 (1995).

¹²G. S. Oehrlein, J. F. Rembetski, and E. H. Payne, *J. Vac. Sci. Technol. B* **8**, 1199 (1990).

- ¹³L. Vallier, J. Foucher, X. Detter, E. Pargon, O. Joubert, G. Cunge, and T. Lill, *J. Vac. Sci. Technol. B* **21**, 904 (2003).
- ¹⁴M. Darnon, T. Chevolleau, T. David, J. Ducote, N. Posseme, R. Bouyssou, F. Bailly, D. Perret, and O. Joubert, *J. Vac. Sci. Technol. B* **28**, 149 (2010).
- ¹⁵M. Darnon, T. Chevolleau, D. Eon, R. Bouyssou, B. Pelissier, L. Vallier, O. Joubert, N. Posseme, T. David, F. Bailly, and J. Torres, *Microelectron. Eng.* **85**, 2226 (2008).
- ¹⁶J. H. Thomas III, C. E. Bryson III, and T. R. Pampalone, *J. Vac. Sci. Technol. B* **6**, 1081 (1988).
- ¹⁷P. J. Cumpson and M. P. Seah, *Surf. Interface Anal.* **25**, 430 (1997).
- ¹⁸S. Tanuma, C. J. Powell, and D. R. Penn, *Surf. Interface Anal.* **21**, 165 (1994).
- ¹⁹C. Powell and A. Jablonski, *Nucl. Instrum. Methods Phys. Res. A* **601**, 54 (2009).
- ²⁰M. P. Seah and S. J. Spencer, *Surf. Interface Anal.* **43**, 744 (2011).
- ²¹W. H. Gries, *Surf. Interface Anal.* **24**, 38 (1996).
- ²²E. Pargon, O. Joubert, N. Posseme, and L. Vallier, *J. Vac. Sci. Technol. B* **22**, 1858 (2004).
- ²³M. P. Seah and S. J. Spencer, *Surf. Interface Anal.* **33**, 640 (2002).
- ²⁴J. Cazaux, *J. Electron Spectrosc. Relat. Phenom.* **178–179**, 357 (2010).
- ²⁵M. P. Seah, *Surf. Interface Anal.* **37**, 300 (2005).
- ²⁶C. Powell and A. Jablonski, *J. Electron Spectrosc. Relat. Phenom.* **114–116**, 1139 (2001).
- ²⁷S. Banna, A. Agarwal, K. Tokashiki, H. Cho, S. Rauf, V. Todorow, K. Ramaswamy, K. Collins, P. Stout, J.-Y. Lee, J. Yoon, K. Shin, S.-J. Choi, H.-S. Cho, H.-J. Kim, C. Lee, and D. Lymberopoulos, *IEEE Trans. Plasma. Sci.* **37**, 1730 (2009).
- ²⁸B. Pelissier, A. Beaurain, J.-P. Barnes, R. Gassilloud, F. Martin, and O. Joubert, *Microelectron. Eng.* **85**, 1882 (2008).